EurJIC
European Journal of Inorganic Chemistry

Minireviews
doi.org/10.1002/ejic.202100031

Chemistry Europe
European Chemical Societies Publishing

Therapeutic and Diagnostic Applications of Multimetallic Rhenium(I) Tricarbonyl Complexes

Zhouyang Huang[a] and Justin J. Wilson*[a]

By virtue of their favorable properties, rhenium(I) tricarbonyl ($Re(CO)_3$) complexes have arisen as novel therapeutic agents and cellular imaging probes for addressing problems of biomedical relevance. Although great success has been found in monometallic complexes of this type, there has been recent interest in developing multimetallic compounds containing $Re(CO)_3$ moieties to capitalize on the potential synergistic effects of different metal centers. This Minireview provides an overview of multimetallic $Re(CO)_3$ complexes that have been developed specifically for biomedical applications. The promising therapeutic and diagnostic potential of such complexes and future needs in this field are discussed.

1. Introduction

Complexes containing the rhenium(I) tricarbonyl ($Re(CO)_3$) core have emerged as promising agents for both therapeutic and diagnostic applications.[1–7] The octahedral geometry, low-spin d^6 electron configuration, and presence of strong-field ligands make this class of compounds kinetically inert, a property that facilitates their use in biology. With respect to their therapeutic applications, $Re(CO)_3$ complexes act via mechanisms of action that are significantly different from those of classical platinum-based chemotherapeutics.[8–15] For instance, our group has described the anticancer activity of a series of tricarbonyl rhenium isonitrile polypyridyl complex (TRIP) complexes.[16–18] TRIP kills cancer cells via the induction of endoplasmic reticulum (ER) stress, marking a notable divergence from the well-established DNA-binding mechanism of Pt(II) chemotherapeutics. Moreover, the rich photophysical properties of the $Re(CO)_3$ core have given rise to promising new photodynamic therapy (PDT) and photoactivated chemotherapy (PACT) agents, owing to their ability to generate singlet oxygen ($^1O_2$) and carbon monoxide (CO) upon irradiation.[19–24]

These same photophysical properties of $Re(CO)_3$ complexes have also been leveraged for diagnostic applications. When diimine ligands with low-lying empty π^* orbitals, such as bipyridine and phenanthroline, are employed as equatorial ligands, the resulting $Re(CO)_3$ compounds are often photoluminescent, owing to the resulting long-lived triplet metal-to-ligand charge transfer (^{3}MLCT) emissive states that are accessible to these complexes. This ^{3}MLCT-based emission has enabled the use of $Re(CO)_3$ complexes for fluorescent cellular imaging.[1,3,4] In addition, $Re(CO)_3$ complexes possess intense vibrational CO stretching modes between 1800–2100 cm^{-1}, a region that is transparent in biological samples. Thus, these compounds have also found applications for vibrational imaging.[25,26] Furthermore, established chemistry has allowed for the synthesis of structurally analogous $^{99m}Tc(CO)_3$ complexes, which can be applied for in vivo single-photon emission computed tomography (SPECT) imaging.[27,28]

Given the valuable therapeutic and diagnostic properties of the $Re(CO)_3$ core, there has been a significant interest in using this fragment in conjunction with other metal centers. Multimetallic complexes, in general, have found useful biological applications because they leverage the distinct properties of different metal centers simultaneously.[29–31] In the context of $Re(CO)_3$ complexes, both homonuclear, which contain multiple Re centers, and heteronuclear, which contain Re and a different metal center, multimetallic compounds have been reported. In this Minireview, we will summarize the therapeutic and diagnostic applications of these $Re(CO)_3$-containing multimetallic complexes. Although other multimetallic complexes of this type have been reported for catalytic applications,[32] we are only focusing on complexes that have been used in a biological setting. Readers are referred elsewhere for reviews on the biological applications of mononuclear $Re(CO)_3$ complexes,[1–7] multimetallic complexes in a more general sense,[29–31] and rhenium complexes where Re exists in oxidation states III, IV, V and VII.[6,33]

2. Homonuclear Complexes

Homonuclear multimetallic $Re(CO)_3$ complexes have attracted significant attention by researchers. The combination of several $Re(CO)_3$ fragments in a single molecule can potentially improve cellular uptake by increasing the lipophilicity or charge,[34] which in turn may enhance both the cytotoxicity and cellular imaging properties. Owing to their relatively straightforward syntheses, the majority of homonuclear $Re(CO)_3$ complexes are linked through axial pyridine-containing ligands. We will discuss these complexes in section 2.1. As the examples below demonstrate, subtle structural alterations, such as changes of bridging groups, linking positions, and axial and equatorial ligands, can

[a] Z. Huang, Prof. Dr. J. J. Wilson
Department of Chemistry and Chemical Biology
Cornell University
Ithaca, NY 14853, USA
E-mail: jjw275@cornell.edu
https://wilson.chem.cornell.edu

Part of the joint "Metals in Medicine" Special Collection with ChemMedChem.

have profound impacts on the biological properties of these pyridyl-bridged homonuclear complexes. In section 2.2, we will discuss non-pyridyl-bridged homonuclear complexes. This class is less common than the pyridyl-bridged systems but exhibits similarly valuable properties.

2.1. Pyridyl-Bridged Complexes

We categorize pyridyl-bridged complexes based on whether they are linked via the *meta*-, *para*-, or *ortho*- position. We found that the *meta*- linked compounds are mainly studied for diagnostic applications, whereas the *para*- linked compounds have been mostly used for therapy. In contrast, the currently reported *ortho*- linked complexes have found less use in biological applications due to their unfavorable antiproliferative properties. Nevertheless, such properties can be potentially beneficial for the design of non-toxic diagnostic probes.

Note that the relationship between the linking position and resulting biological properties is currently not well understood. Further studies on the structure-activity relationships are needed for the rational design of this class of compounds.

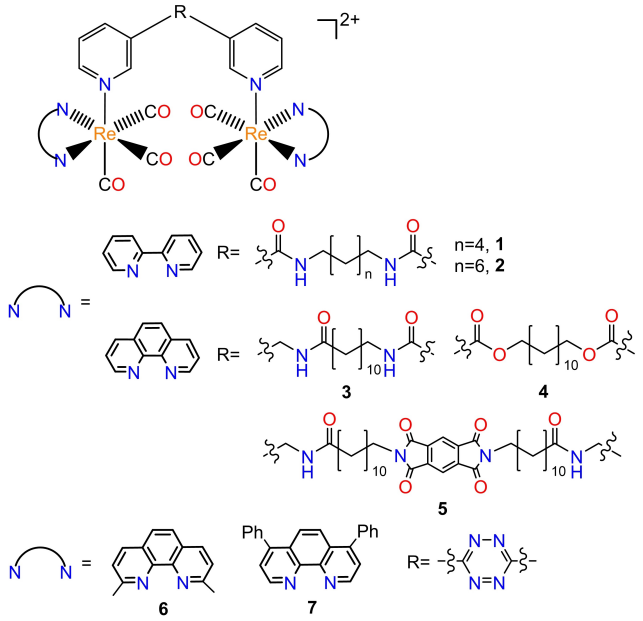

Figure 1. Structures of *meta*- linked pyridyl-bridged homonuclear compounds (**1**–**7**).[34,35]

2.1.1. Linking through the Meta-Position

As an early example of the pyridyl-bridged homonuclear complexes, a library of dinuclear $Re(CO)_3$ complexes tethered together with aliphatic chains of different lengths (**1**–**5**) were investigated in biological systems (Figure 1).[34] In live cell-imaging experiments, all of these complexes were shown to be taken up efficiently by MCF-7 cells via non-energy dependent mechanisms. The extent of uptake and intracellular localization depend on both the chain lengths and nature of the linkage. For example, the diamide-linked compound **3** and pyromellitate-linked compound **5** show a distinctive pattern of staining of the organelles within the cytoplasm, whereas the diester-linked compound **4** exhibits nucleolar localization with the greatest intracellular photoluminescence intensity among all complexes. The good cellular uptake, bright photoluminescent emission, and low toxicity of these complexes render them favorable as intracellular phosphorescent imaging probes for MCF-7 cells.

The functionalities of these homonuclear compounds can be tuned by using different linkers between the two pyridyl ligands. To enable their use as bioorthogonal imaging probes, a 1,2,4,5,-tetrazine was employed as the bridge in compounds **6** and **7** (Figure 1).[35] This linker reacts rapidly with dienophiles[36] such as 5-norbornen-2-ol (NBO) and (1R,8S,9 s)-bicyclo[6.1.0] non-4-yn-9-ylmethanol (BCN), via the inverse electron-demand Diels-Alder cycloaddition. This reactivity can be leveraged for the labelling of biomolecules such as bovine serum albumin (BSA). When incubated with BSA lacking a biorthogonal BCN tag, **6** and **7** were poorly emissive due to quenching by the bridging tetrazine. However, a significant emission enhancement was observed when **7** was incubated with BCN-modified BSA (Figure 2), triggering the conversion of the bridging tetrazine to the corresponding pyridazine product and covalently attaching the $Re(CO)_3$ complex to the protein. Notably, the reaction kinetics for this process are faster in **6** and **7** compared to their mononuclear counterparts and free

Zhouyang Huang obtained a B.S. in Chemistry at the University of California, Santa Barbara (2018), where he carried out undergraduate research in the laboratory of Prof. Trevor W. Hayton on the topic of copper hydride complexes. Zhouyang obtained his M.S. degree in Inorganic Chemistry from Cornell University (2020) and is currently a Ph.D. student under the supervision of Prof. Justin J. Wilson. His project focuses on the use of rhenium and ruthenium complexes for biological applications.

Justin Wilson earned a B.S. in Chemistry at the University of California, Berkeley in 2008 and a Ph.D. in Inorganic Chemistry at the Massachusetts Institute of Technology in 2013. Following his stay as a Seaborg Institute Postdoctoral Fellow at Los Alamos National Laboratory, Justin joined the Department of Chemistry and Chemical Biology at Cornell University in Ithaca, New York, as an assistant professor. Projects in his group span several topics within medicinal inorganic chemistry, including metal-based anticancer agents, novel ion channel inhibitors, and chelators for nuclear medicine.

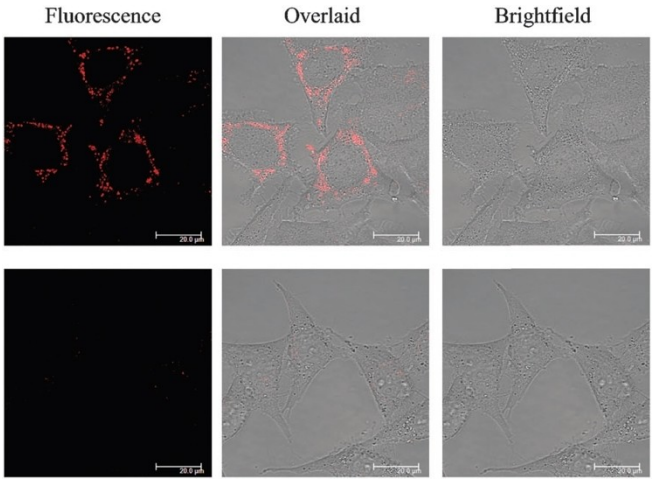

Figure 2. Confocal fluorescence microscopy images of live HeLa cells that have been incubated with BSA–BCN (top) and unmodified BSA (bottom), respectively, and subsequently with compound **7**. Reproduced from ref.,[35] Copyright (2015), with permission from the Royal Society of Chemistry.

ligands, suggesting that the presence of both cationic $Re(CO)_3$ cores activates the tetrazine.

2.1.2. Linking through the Para-Position

Many *para*- linked pyridyl-based homonuclear complexes have been studied for their anticancer activities. For example, dinuclear compounds tethered with ethyl groups (**8** and **9**) have been investigated in biological systems (Figure 3).[37] Compared to *meta*- linked complexes **1**–**5**, compounds **8** and **9** exhibit distinct intracellular localization and anticancer properties. The less lipophilic compound **8** localizes to lysosomes and induces caspase-independent apoptosis, whereas the more lipophilic compound **9** accumulates in mitochondria and induces caspase-independent paraptosis (Figure 4). These results demonstrate how slight structural changes can have large effects on the biological properties and applications of this class of compounds. Furthermore, both **8** and **9** are more cytotoxic than their mononuclear counterparts. However, when evaluated on a per Re basis, compound **9** is only 0.8 to 2.3 times more potent than its mononuclear counterpart, suggesting that the effect of having the second Re center is additive. By contrast, compound **8** is several orders of magnitude more potent than its mononuclear form, suggesting a synergistic effect.[5]

Biological properties of these homonuclear compounds can also be modified by using different equatorial ligands. In compounds **10** and **11**, carboline derivatives were employed as equatorial ligands (Figure 3).[38] Both compounds appeared to localize to lysosomes. Complex **11** was found to cause lysosome damage in A549 cells, owing to its ability to produce reactive oxygen species (ROS) like superoxide ($O_2^{\bullet-}$) and hydrogen peroxide (H_2O_2). In addition, both complexes are efficient singlet oxygen ($^1O_2$) sensitizers. Such property confers **10** and **11** with significant photocytotoxic properties. Irradiation of cells treated

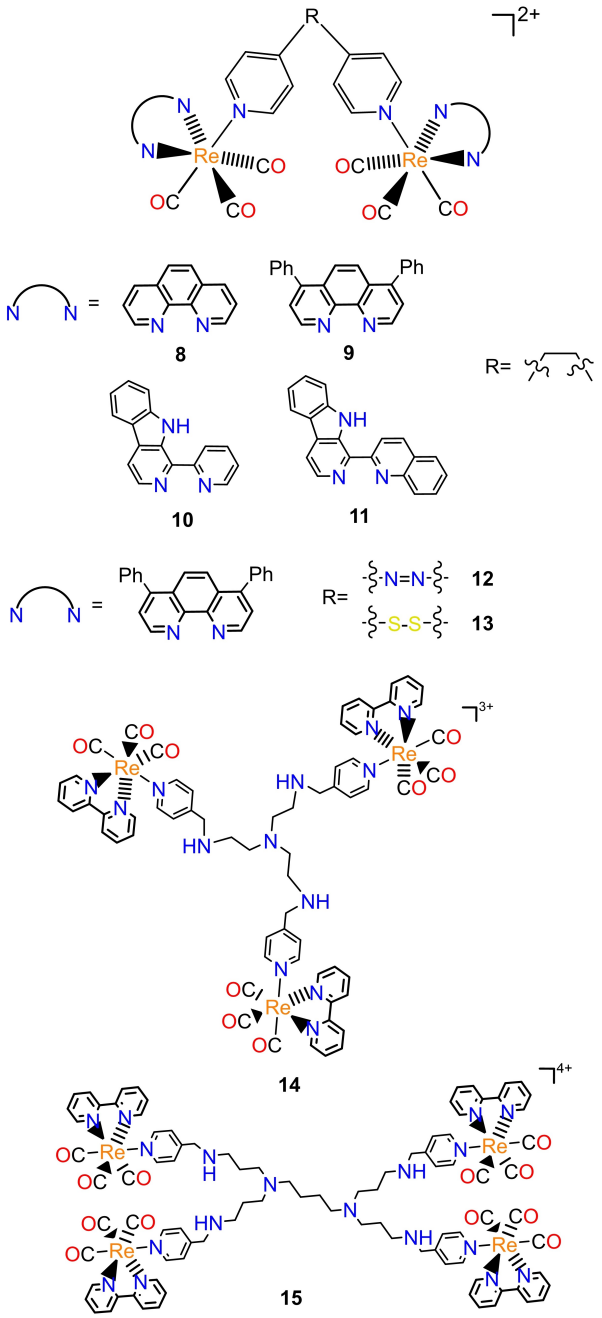

Figure 3. Structures of *para*- linked pyridyl-bridged homonuclear compounds (**8**–**15**).[3–40]

with these compounds using 425 nm light gives rise to potent cytotoxic effects, as reflected by phototoxicity index values of 60.8 and 41.8 for **10** and **11**, respectively. This study demonstrates the potential of such compounds as lysosome-targeting PDT agents.

As shown in the previous subsection, the choice of linkers between the two pyridyl ligands can influence the functionalities of the resulting homonuclear compounds. Azo and disulfide groups, which can react with reductants, are employed as linkers in compound **12** and **13**, respectively (Figure 3).[39] Addition of glutathione, a common biological reducing agent,

to both complexes led to the cleavage of the azo and disulfide bonds, presumably generating the corresponding bioactive mononuclear fragments. This favorable redox reactivity of **12** and **13** can be leveraged for hypoxic activation of these complexes in cancer cells. Furthermore, both compounds accumulate in mitochondria and cause oxidative stress and mitochondrial dysfunction. Moreover, both complexes kill cancer cells by inducing necroptosis and caspase-dependent apoptosis simultaneously. In vivo studies show that compound **12** and **13** are able to inhibit tumor growth in nude mice bearing carcinoma xenografts.

Trimeric (**14**) and tetrameric homonuclear complexes (**15**) have also been investigated for their anticancer properties (Figure 3).[40] Although the 50% growth inhibitory concentration (IC_{50}) values of **14** and **15** are lower than those of their mononuclear analogues, when these values are normalized per Re atom, the cytotoxicity of complex **14** and **15** is either the same as or worse than their mononuclear forms. Thus, for these compounds, the effect of multinuclearity is additive instead of synergistic.

Additional bridging ligands in the equatorial positions are also possible. A large library of complexes of this type was studied for their anticancer activities (**16**–**37**) (Figure 5).[41–44] An early example is a library of metallacyclophanes with ester linkages (**16**–**20**). Within this class of compounds, those containing longer alkyl chains exhibit higher cytotoxicity (**16** < **18** < **20**).[41] A similar trend was observed in amide-linked[42] (**21** < **22** < **23** < **24**) and oxamidato-linked[43] (**25** < **26** < **27** < **28** < **29**) compounds, suggesting that flexibility is important for modulating the biological activities of these complexes. Chalcogenolato-bridged compounds (**30**–**37**) are generally less potent than the aforementioned complexes, with the exceptions of **31** and **33**, which display significant cytotoxicity against Hep G2 cells.[44] Compound **24** is the most potent complex among these equatorially linked complexes, with cytotoxicity profiles similar to cisplatin. The longer, more flexible alkyl chain (n = 8) may contribute to its high activity. Moreover, morphological analyses of cells treated with these compounds suggest that complexes **20**, **24**, **25**, **29**, **31**, and **33** kill cancer cells via the induction of apoptosis. Notably, compound **16**, **18**, and **20**–**29** exhibit selectivity towards cancer cells over PMBCs (normal blood) cells, indicating that they may have a favorable therapeutic index for future in vivo studies.

2.1.3. Linking through the Ortho-Position

Although a few *ortho*-pyridyl linked homonuclear complexes have been reported, their antiproliferative properties are not as favorable as those of their *para*- analogues. Compound **38** is a dirhenium complex bridged by a tertiary amine group attached to *ortho*- positions of two pyridyl rings and *meta*- position of one bipyridyl ring (Figure 6).[45] This complex exhibits weak activity against multiple cancer cell lines (IC_{50} > 180 μM).

A systematic family of equatorially bridged dirhenium complexes has been studied for their antimicrobial properties (Figure 7).[46] These complexes (**39**–**50**) employ bidentate 2-

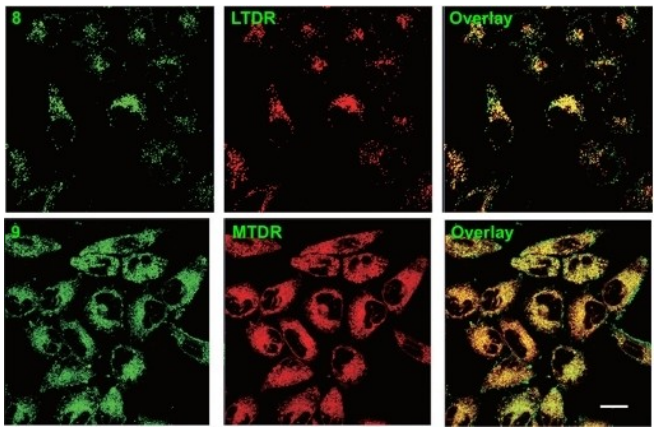

Figure 4. Top: Confocal fluorescence microscopy images of HeLa cells co-labelled with **8** (20 μM, 2 h) and LysoTracker Deep Red FM (LTDR) (50 nM, 0.5 h). Bottom: Confocal microscopy images of HeLa cells co-labelled with **9** (20 μM, 2 h) and MitoTracker Deep Red FM (MTDR) (150 nM, 0.5 h). Scale bar: 20 μm. Adapted from ref.[37]

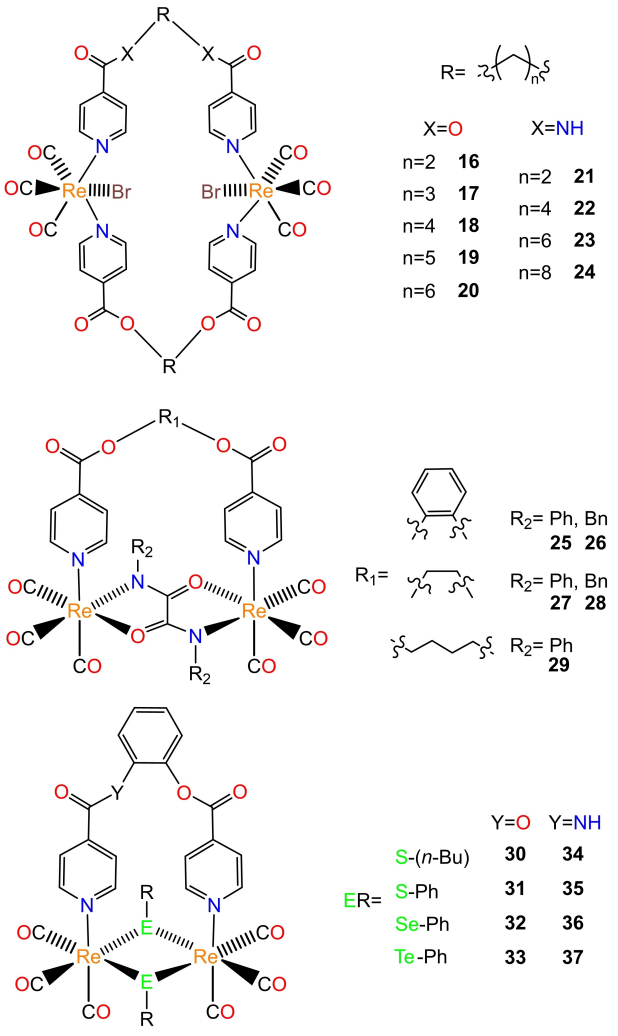

Figure 5. Structures of *para*- linked pyridyl-bridged homonuclear compounds (**16**–**37**).[41–44]

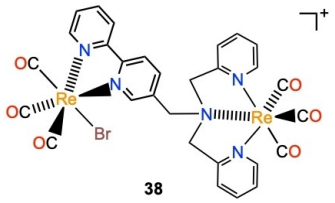

Figure 6. Structure of *para*- linked pyridyl-bridged homonuclear compound **38**.[45]

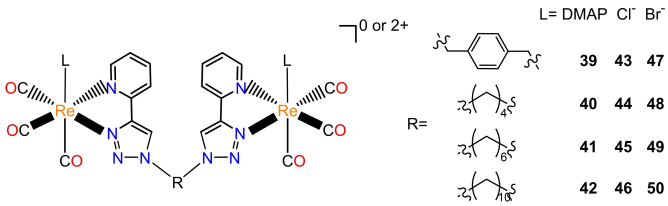

Figure 7. Structures of *para*- linked pyridyl-bridged homonuclear compounds **39**–**50**.[46]

pyridyl-1,2,3-triazole ligands that are attached with different alkyl or aryl linkers. The axial ligands are either 4-dimethylaminopyridine (DMAP) (**39**–**42**), chloride (**43**–**46**), or bromide (**47**–**50**). In general, the cationic complexes bearing the DMAP ligand (**39**–**42**) are more active than the neutral complexes (**43**–**50**) against both Gram-positive (*S. aureus*) and Gram-negative (*E. coli*) microorganisms, presumably due to their greater lipophilicity and charge. Nevertheless, these complexes are unlikely to be used as antimicrobial agents because of their modest minimum inhibitory concentrations (16–1024 $\mu g\,mL^{-1}$).

2.2. Non-Pyridyl-Bridged Complexes

The structural versatility of $Re(CO)_3$ complexes has also enabled the development of homonuclear compounds with a diverse range of non-pyridyl ligands that can span either axial or equatorial positions on the complexes. For instance, complex **51** is bridged by *N*′-[1-(2-oxo-2H-chromen-3-yl)-ethylidene]-hydrazinecarbodithioic acid benzyl ester (Figure 8).[47] In this

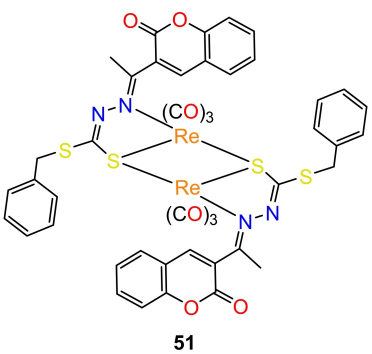

Figure 8. Structure of non-pyridyl-bridged homonuclear compound **51**.[47]

complex, the bridging ligand occupies both an equatorial and axial site on the Re center. This complex was found to have similar cytotoxic activity as the established breast cancer drug tamoxifen.

Rigid dinuclear $Re(CO)_3$ complexes assembled from two bridging chloride ligands and a bridging pyridazine ligand have been developed as a template for bioimaging agents because of their low-toxicity and good photoluminescent properties.[48] The bridging pyridazine ligand, in particular, provides a useful attachment point for the conjugation of different biological targeting vectors. This strategy has been employed to attach peptide nucleic acids (PNAs) to this dirhenium core to target it to DNA in cells (**52** and **53**) (Figure 9).[49] Compound **53** can be excited by two-photon absorption using near-IR laser light, which more effectively penetrates biological tissue and causes less damage than the corresponding use of single photons in the near-UV region. Moreover, **53** can stain both the cytoplasm and nucleus of HEK-293 cells. Within the nucleus, the compound is detected more readily within the blue channel (485 nm), indicating that the emission energy of this compound depends on its local environment (Figure 10). The blue-shift of emission in the nucleus is attributed to the reduced mobility

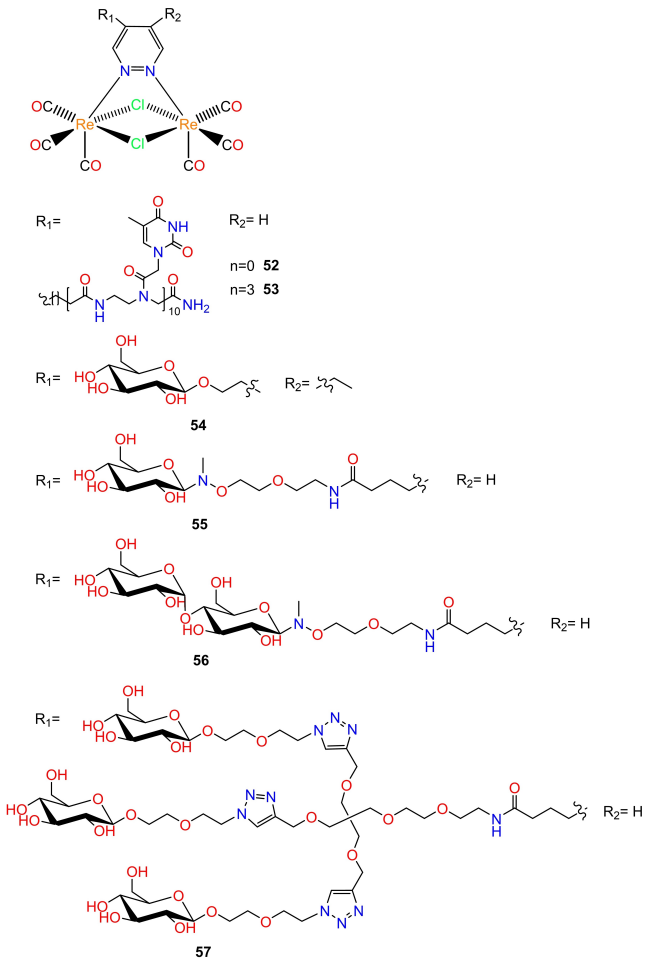

Figure 9. Structures of non-pyridyl-bridged homonuclear compounds **52**–**57**.[48,49]

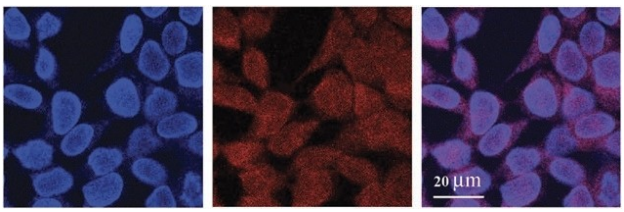

Figure 10. Fluorescence microscopy images of HEK-293 cells stained with **53**, recorded about 10 min after the addition of the complex, through a 485/30 (left) and a 600/40 nm (center) band pass filter and their superposition (right). Reproduced from ref.[49] Copyright (2010), with permission from the Royal Society of Chemistry.

and more hydrophobic character of the nuclear environment, in comparison with the cytoplasm.

In addition to PNAs, glucose has also been attached to this dirhenium moiety via the pyridazine bridging ligand (**54**–**57**). For these complexes, the glucose was used to enhance both their aqueous solubilities and cellular uptake.[48] Fluorescence microcopy imaging of **54**–**56** in HeLa cells shows that they are internalized effectively and localize preferentially to the endoplasmic reticulum (ER). The efficient cell uptake, good organelle selectivity, and low cytotoxicities of this class of complexes demonstrate that they are valuable phosphorescent imaging probes.

Higher order homonuclear $Re(CO)_3$ clusters have also been assembled and evaluated for biological activity. For example, a tetrarhenium complex (**58**), which is linked by a central porphyrin with four terminal 1,4,7-triazacyclononane (TACN) ligands that bind to the $Re(CO)_3$ cores, has been reported (Figure 11).[50] Based on the established photodynamic therapeutic properties of porphyrins and related molecules,[51–53] the phototoxicity of **58** was examined. Notably, the cytotoxicity of **58** in HeLa cells can be enhanced up to 71-fold when irradiated by red light, presumably via the generation of $^1O_2$. Moreover, the photoactivity of the free tetrafunctionalized porphyrin is enhanced upon coordination to Re, showing the benefits of including this metal in the structure. In addition, DNA-binding studies show that **58** selectively interacts with quadruplex DNA. Because quadruplex DNA is found in a number of oncogenes within the telomeric regions of the genome,[54] this binding interaction may confer **58** with greater cancer-targeting properties.

All the compounds discussed above employ bridging ligands containing nitrogen donors; homonuclear complexes linked by ligands using alternative donors have also been studied. A dinucleating bidentate equatorial phosphine ligand was used to assemble complex **59** (Figure 11).[55] The hydroxide-bridged trinuclear and dinuclear (**60** and **61**) assemblies have also been reported (Figure 11).[56] All three complexes display similar cytotoxic activity against various cancer cell lines.

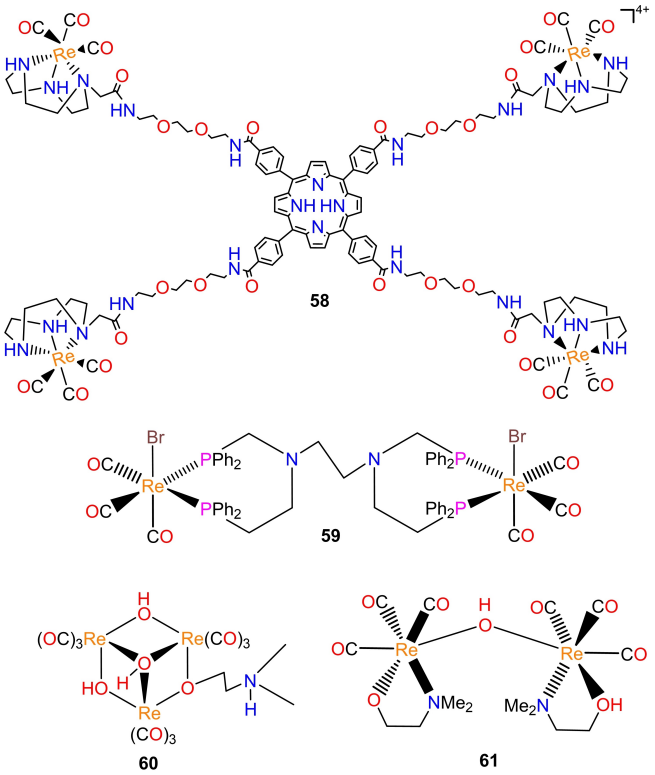

Figure 11. Structures of non-pyridyl-bridged homonuclear compounds **58**–**61**.[50,55,56]

3. Heteronuclear Complexes

There has been a considerable interest in developing heteronuclear complexes for biological applications, because such compounds can leverage functionalities of different metallic fragments simultaneously. In the context of $Re(CO)_3$-based heteronuclear complexes, the Re fragment can be employed either as a diagnostic or therapeutic component, owing to its favorable photophysical and biological properties. In this section, we will discuss heterometallic complexes of Re conjugates with first-, second-, and third-row transition metals, as well as rare earth elements.

3.1. First-Row Transition Metals

There are five first-row transition metals that are essential to human health: manganese, iron, cobalt, copper, and zinc.[57] Three of these—manganese, iron, and cobalt—have been conjugated to $Re(CO)_3$ complexes for evaluation of their antimicrobial, anticancer, and cellular imaging applications. These complexes fall into one of the two classes: 1) first-row metallocene conjugates and 2) cobalamin conjugates.

3.1.1. Metallocene Conjugates

Metallocenes, particularly ferrocene derivatives, have found use in various biological applications, including as potent anticancer and antimicrobial agents.[58] Multimetallic complexes comprising a metallocene and $Re(CO)_3$ core have the potential for enhanced bioactivity and may be less susceptible to drug resistance mechanisms. For these reasons, trimetallic (**62** and **63**)[59] and bimetallic (**64** and **65**)[60] metallocene-containing compounds were synthesized (Figure 12). These compounds contain a $Re(CO)_3$ fragment chelated by a dipicolylamine group linked to either a ferrocene (Fc) or ruthenocene (Rc) moiety, and a $[CpMn(CO)_3]$ (Cy, where Cp = cyclopentadienide) fragment. All four of these complexes were investigated for their antimicrobial properties. Among these four compounds, it was noteworthy that the activity of **62** against MRSA (methicillin-resistant *Staphylococcus aureus*) is 90 times greater than that of amoxicillin, a commercially used antibacterial agent. Additionally, mechanistic studies revealed that **62** targets the bacterial membrane and induces oxidative stress. The less potent derivatives (**63**–**65**) also target the bacterial membrane. Control experiments showed that the antimicrobial activity of these compounds was largely retained in the corresponding mononuclear Re fragment, suggesting that the $Re(CO)_3$ moiety, rather than the trimetallic entity, is the crucial component that is responsible for the antibacterial activity of these compounds.

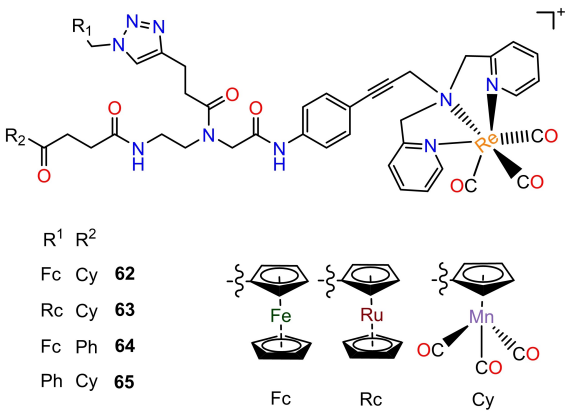

Figure 12. Structures of metallocene conjugates **62**–**65**.[59,60]

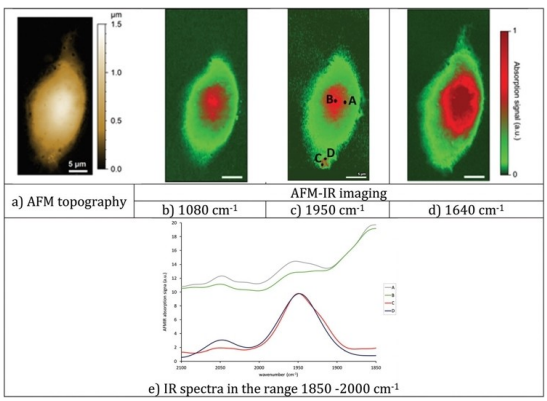

Figure 14. Top: Images and IR mapping of one MDA-MB-231 cell incubated 1 h at 37 °C in the presence of 10 μM of **70**. (a) AFM topography, (b–d) AFM-IR images at: (b) 1080 cm^{-1} (phosphate); (c) 1950 cm^{-1} ($Re(CO)_3$) of (**70**); (d) 1640 cm^{-1} (Amide I). Bottom: (e) Superimposition of AFM-IR spectra, in the 1850–2000 cm^{-1} range of different spots highly absorbing at 1950 cm^{-1}. A and B: spots in the region attributed to cell nucleus, C and D: spots corresponding to a precipitate of **70** present on the cell surface. Reproduced from ref.,[62] Copyright (2018), with permission from the Royal Society of Chemistry.

Re$(CO)_3$ has also been attached to Fc for designing new anticancer agents. For example, the aldimine-linked Fc–Re conjugates, **66** and **67** (Figure 13), have been studied, operating under the hypothesis that the two metallic fragments can act synergistically.[61] Notably, **67** exhibits cytotoxicity greater than cisplatin in both breast cancer MDA-MB-231 and colon cancer HCT-116 cells. By contrast, **66** is less active, thus demonstrating how subtle structural differences in these complexes can have significant effects on biological activities.

Conjugation with other Fc derivatives has also been explored. Ferrocifen, an analogue of the established anticancer drug tamoxifen that contains ferrocene in place of a phenyl ring, is a promising anticancer drug candidate that exhibits potent activity both in vitro and in vivo.[63] However, fluorescent cellular imaging of this class of compounds is difficult due to the strong ability of ferrocene to quench luminescence.[64] To track the intracellular localization of ferrocifen, a $Re(CO)_3$ tag was conjugated to this molecule via different positions (**68**–**70**) (Figure 13).[62] The intense IR absorption band of the CO stretching mode of the $Re(CO)_3$ core, which resonates within the biological transparent region of 1800 to 2100 cm^{-1}, can be used for IR imaging in cells. Atomic force microscope infrared-spectroscopy (AFM-IR) imaging of **70** has been conducted in MDA-MB-231 cells. The carbonyl stretching bands of the $Re(CO)_3$ moiety at 1950 cm^{-1} of **70** colocalize strongly with amide and phosphate vibrational modes, indicating that this compound preferentially accumulates in the nucleus (Figure 14). Despite the value of these IR microscopy studies, the

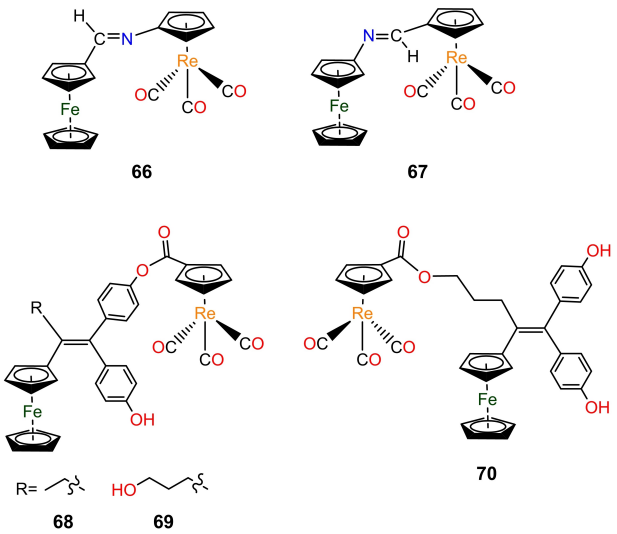

Figure 13. Structures of metallocene conjugates **66**–**70**.[61,62]

conjugation of the $Re(CO)_3$ core to ferrocifen significantly reduces the cytotoxic activity of the parent drug candidate, suggesting that the interpretation of these IR microscopy studies with large IR labels should be taken with caution.

3.1.2. Cobalamin Conjugates

Cyanocobalamin (vitamin B12) is an essential nutrient for most living organisms. It plays a key role in a diverse range of enzymatic processes.[65] In particular, cancer cells have a high demand for vitamin B12 for proliferation, which makes cobalamin an attractive cancer-targeting agent.[66] For these reasons, cyanocobalamin (vitamin B12) was conjugated to a $Re(CO)_3$ compound to yield complexes **71** and **72** (Figure 15).[67] These complexes differ by the nature of the attachment point, with complex **71** linked with an axial nitrile donor and complex **72** conjugated via an axial pyridine ligand. Although complex **71** was found to be unstable in cell media, both complexes exhibit in vitro anticancer activities, as evidenced by their low μM IC_{50} values in PC-3 prostate cancer cells. Because the ^{3}MLCT photoluminescence of the $Re(CO)_3$ moiety is quenched by cyanocobalamin, IR microscopy of cells treated with **72** was used to probe its intracellular localization. These studies show that **72** accumulates in the cytoplasm and perinuclear regions of the cell.

3.2. Second-Row Transition Metals

Technetium and its neighbor ruthenium are the two second-row transition metals that have been conjugated to $Re(CO)_3$ complexes for biological applications. Both Tc and Ru complexes have been used widely for diagnostic purposes owing to their unique nuclear and photophysical properties, respectively. In this section, we will discuss the heterometallic complexes of $Re(CO)_3$ and these two metal ions, as well as their biological applications for cellular imaging, anticancer therapy, and pH sensing.

3.2.1. Technetium Conjugates

^{99m}Tc is used extensively for SPECT imaging.[27,28] There has been an interest in developing dual-imaging probes that integrate the high sensitivity of nuclear imaging, like SPECT, with the good spatial resolution of fluorescence imaging. To this end, the Re–Tc conjugates **73**[68] and **74**[69] were prepared to combine the photoluminescent properties of the $Re(CO)_3$ core with the gamma emission properties of the $^{99m}Tc(CO)_3$ fragment (Figure 16). Both **73** and **74** are stable in the presence of a large molar excess of histidine, indicating their biocompatibility. In addition, they are photoluminescent with good quantum yields. Compound **74** is mostly non-toxic in A549, HT29, and MCF-7 cells, and its emission can clearly be detected at the cellular level, demonstrating its potential as a diagnostic probe.

3.2.2. Ruthenium Conjugates

Similar to those of Re, Ru complexes have emerged as promising agents for both therapeutic[70] and diagnostic[71] applications, owing to their favorable photophysical and biological properties. Because integrating these two metal centers together may produce synergistic effects, multiple Re–Ru conjugates have been reported. Compound **75** is an early example combing $[Ru(NN)(dppz)]^{2+}$ (NN = polypyridine ligands, dppz = dipyrido[3,2-a:2′,3′-c] phenazine) with $[Re(CO)_3(dppz)]^+$ (Figure 17).[72] Complexes of the general formula $[Ru(NN)_2(dppz)]^{2+}$ have been demonstrated to be "DNA light switches," which undergo a significant increase in photoluminescence upon binding to DNA via intercalation.[73,74] By contrast, the Re analogue of this compound $[Re(CO)_3(dppz)]^+$ is a "DNA scissor", which intercalates with DNA but triggers photocleavage upon irradiation.[75,76] The combination of these two moieties yielded the theranostic complex **75**, which displays both DNA light switch and cleavage properties. A related analogue complex **76**, which contains a longer alkyl chain linker between the Ru and Re fragments, has also been prepared and studied (Figure 17).[77] The longer alkyl chain linker of **76** gives rise to improved cellular delivery and nuclear-targeting properties compared to **75**, thus highlighting the important role of the bridging group for this class of molecules. Furthermore, the optimal cellular uptake, localization, and

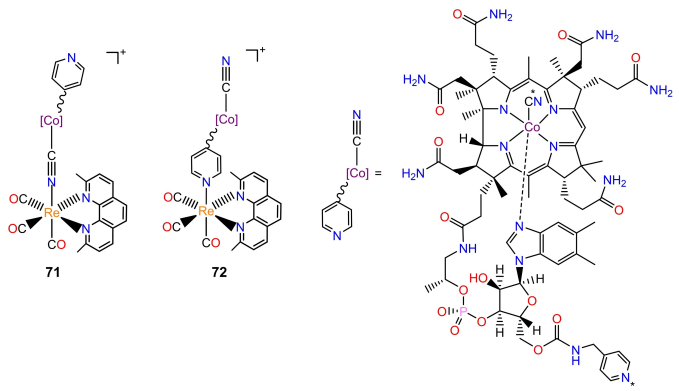

Figure 15. Structures of cobalamin conjugates **71** and **72**.[67]

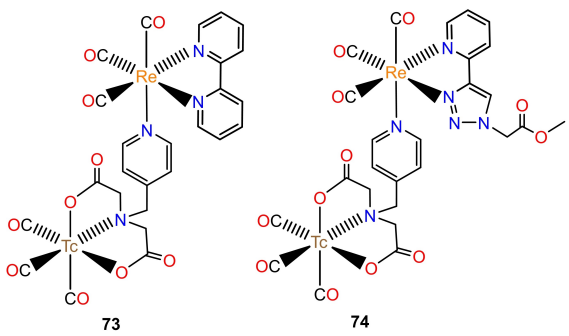

Figure 16. Structures of technetium conjugates **73** and **74**.[68,69]

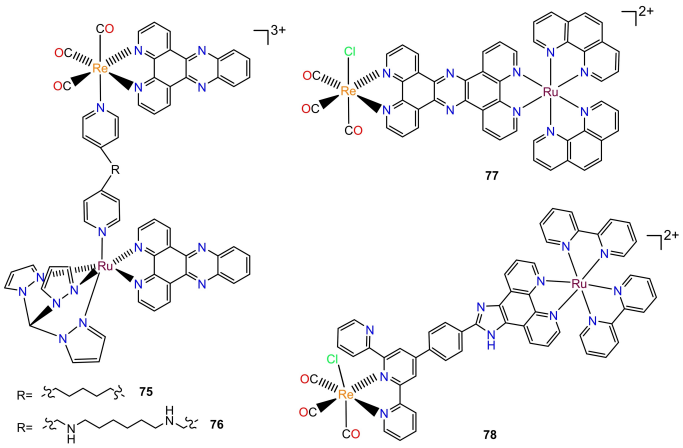

Figure 17. Structures of ruthenium conjugates **75**–**78**.[72,77–79]

photophysical properties of **76** enabled it to be used as a probe for stimulated emission depletion (STED) microscopy, a super-resolution imaging technique.

Following this line of research, another DNA light switch Ru compound, $[Ru(bpy)_2(tpphz)]^{2+}$ (tpphz = tetrapyridyl[3,2-a:2′,3′-c:3″,2″-h:2‴,3‴-j]-phenazine), was attached to a $Re(CO)_3$ fragment in complex **77** (Figure 17).[78] In this compound, the Re and Ru fragments are linked via the equatorial tpphz ligand, rather than the alkyl chain linkages employed for **75** and **76**. As opposed to the parent complex, which binds to DNA via intercalation, **77** interacts with this biomolecule through minor groove binding. Although the cytotoxicity of **77** towards A2780 ovarian cancer cells and cisplatin-resistant A2780CIS ovarian cancer cells is less than that of the mononuclear Ru(tpphz), the heteronuclear compound was able to circumvent the cisplatin-resistance mechanisms more effectively.

The dual luminophore properties of dinuclear Re–Ru complexes have also been investigated to develop a pH sensor. In particular, complex **78** (Figure 17), linked by terpyridine functionalized imidazo [4,5-f]-1,10-phenanthrolines, acts as a highly efficient pH-induced novel "off-on-off" luminescence switch (Figure 18).[79] When pH is below 0.40, the luminescence of the complex was quenched due to the protonation of the imidazole ring. When pH was raised from 0.40 to 4.22, the emission intensity of **78** increased by a factor of 31 due to the deprotonation of the positively charged imidazole ring. When pH was increased from 4.22 to 10.80, the emission intensity of **78** decreased by a factor of 15, owing to the deprotonation of the neutral imidazole ring. It also exhibits a "turn-on" response to $H_2PO_4^-$ and a "turn-off" response to F^- and OAc^-. Lastly, this compound exhibits only minimal cytotoxicity in HeLa cells, thereby increasing its value for sensing and cellular imaging applications.

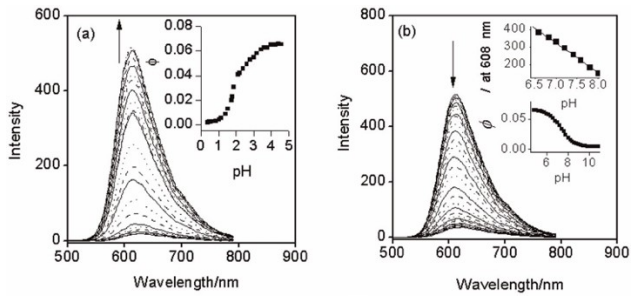

Figure 18. Changes of emission spectra (λ_{ex} = 460 nm) of **78** (10 μM) upon raising pH from 0.40 to 5.00 (a) and from 5.00 to 10.00 (b) Reproduced from ref.,[79] Copyright (2014), with permission from the Royal Society of Chemistry.

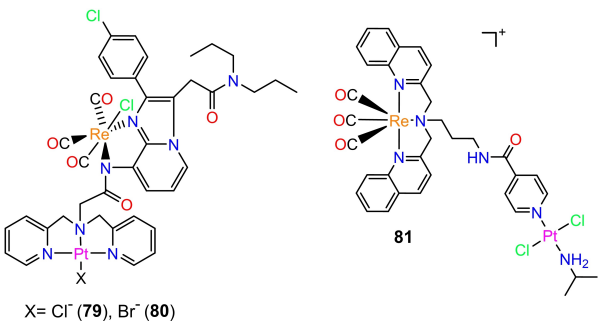

Figure 19. Structures of platinum conjugates **79**–**81**.[81,82]

3.3. Third-Row Transition Metals

Moving to the third-row, platinum and gold, two noble metals that have a long history in the field of medicine, have been attached to $Re(CO)_3$ cores to develop new anticancer agents. In this section, we will discuss the effects of Re on the biological properties of these Au and Pt heterometallic conjugates.

3.3.1. Platinum Conjugates

The clinical success of cisplatin and related platinum-based drugs has sparked many efforts to develop improved anticancer agents containing this element.[80] One promising direction in this field is to combine platinum with other metal ions to explore potential synergistic effects. In this context, several Re-Pt conjugates have been studied. For instance, Re-Pt complexes linked by the ligand CB256 (**79** and **80**) have been reported (Figure 19).[81] CB256 binds to translocator protein (TSPO), a mitochondrial protein that is highly expressed in cancers and is associated with a wide range of biological processes including cell proliferation, apoptosis, and immunomodulation. In these constructs, a Pt(II) center is chelated by the dipicolylamine group of CB256, and the $Re(CO)_3$ fragment is attached directly to donors on the TSPO-binding part of the molecule. Compounds **79** and **80**, which only differ based on the halide ligand that is bound to the Pt(II) center, are taken up by cancer cells much more effectively than their mononuclear counterparts, cisplatin and $[ReBr(CO)_3(OH_2)_2]$. Compared to free CB256, however, the affinity of **79** and **80** for TSPO is reduced more than 3-fold. Furthermore, the cytotoxicity of the conjugates against cancer cells is also much lower than both CB256 and

cisplatin, indicating that this heterodinuclear complex does not confer any advantages over the free organic component.

Another pharmaceutical agent, namely deferasirox, an orally available iron chelator used to treat iron overload, has also been used to form dinuclear Re-Pt complexes (**82**–**86**) (Figure 20).[83] In these constructs, the coordination spheres of the Pt(II) and $Re(CO)_3$ cores are completed by different monodentate chelating components of deferasirox. All compounds are stable in aqueous solution and stable in the presence of Fe^{3+}, indicating that the bridging ligand is unlikely to be displaced under biological conditions. Compound **86**, which contains a triphenylphosphine ligand on the Pt(II) center and a pyridine ligand on the $Re(CO)_3$ center, is the most cytotoxic compound in this class. It is tenfold more active than cisplatin in MDA-MB-231, MCF-7, and A2780 cancer cells, but **86** is overall less cytotoxic than the free ligand, deferasirox.

Re-Pt complexes have also been studied in the context of photodynamic therapy. The Re-Pt complex **81** contains a $Re(CO)_3$ core chelated to bisquinoline ligands attached to a Pt(II) complex with *trans*- leaving groups (Figure 19).[82] The bisquinoline-$Re(CO)_3$ fragment has previously been shown to sensitize the generation of singlet oxygen and act as a photodynamic therapeutic agent.[8][20] Likewise, upon irradiation of cells treated with **81**, an up-to-7-fold enhancement in cytotoxicity is observed, rendering this compound more potent than cisplatin in HeLa and cisplatin-resistant A2780R cancer cell lines.

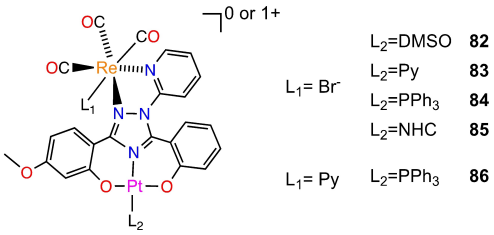

Figure 20. Structures of platinum conjugates **82**–**86**.[83]

3.3.2. Gold Conjugates

Gold(I) complexes have a long history in the field of medicine but have recently received renewed interest by the research community.[84,85] For example, auranofin, a Au(I)-based drug that has been approved for the treatment of arthritis, has also been shown to possess interesting anticancer activities.[86] To leverage the imaging properties of the $Re(CO)_3$, a large series of Re-Au complexes (**87**–**104**) has been prepared and investigated for biological activity.[87–90] Complexes **87**–**89** (Figure 21) contain an alkynyl Au(I) unit that binds to the $Re(CO)_3$ core through a nitrogen donor. By contrast, **90** (Figure 21) contains a Au(I) core that is bound to phosphine and imidazole donors.[87] Compounds **87**–**90** are over 10 times more cytotoxic than their mononuclear Re counterparts, suggesting that gold is the main source of cytotoxicity. Moreover, **87**–**89** are more cytotoxic than **90**, indicating the importance of the alkynyl fragments on mediating the biological activity of the Au(I) center. Confocal fluorescence microscopy studies show that **87**–**90** localize to the nucleus, whereas their mononuclear Re counterparts do not. This result highlights the role of Au fragments in influencing the cellular localization of Re-Au conjugates. In addition, morphological analyses suggest that cell death might be due to both apoptosis and necrosis for compounds **87**–**90**.

For complexes **91**–**93** (Figure 21),[88] the linear Au(I) moiety is bound to a chloride ligand and a phosphine containing a flexible alkyl chain with a nitrogen donor that is coordinated to the axial position of the $Re(CO)_3$ core. The cytotoxicity of **91**–**93** is very similar to that of their mononuclear gold analogues, suggesting that Au is still the main source of their biological activities. In substituting the chloride ligands of **91**–**93** with another ditopic phosphine-nitrogen donor ligand, the heterotrimetallic complexes **94**–**96** (Figure 21), which contain two $Re(CO)_3$ and one Au(I) centers, were obtained. Compared to the dinuclear complexes **91**–**93**, these trimetallic complexes exhibit enhanced cytotoxicity against cancer cells. The greater efficacy of **94**–**96** was attributed to their higher charges and lipophilicities, as opposed to the intrinsic cytotoxic effects of the additional $Re(CO)_3$ fragment. In addition, fluorescence microscopy was used to image both **94** and **95** in A549 lung cancer cells, revealing that these compounds exhibit a nonuniform cytoplasmic distribution. Moreover, both complexes display some DNA accumulation, which was confirmed by a colocalization experiment using DRAQ5, a fluorescent nuclear DNA dye.

Analogous to compounds **87**–**89**, complexes **97**–**99** bear a Au(I) alkynyl phosphine fragment attached to the axial position of the $Re(CO)_3$ core via a nitrogen donor (Figure 22).[89] However, in place of the supporting equatorial bipyridine ligands, bidentate pyridyl *N*-heterocyclic carbene (NHC) ligands were employed. Compounds **97**–**99** exhibit antiproliferative activity against A549 cells, whereas their mononuclear Re counterparts are mostly non-toxic. This result is consistent with the other Re-Au conjugates discussed above, where the Au(I) fragment appears to play a larger role in mediating their cytotoxic effects.

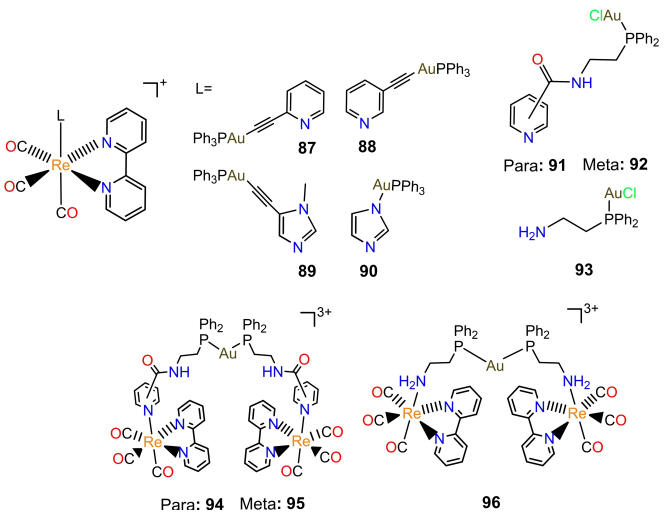

Figure 21. Structures of gold conjugates **87**–**96**.[87,88]

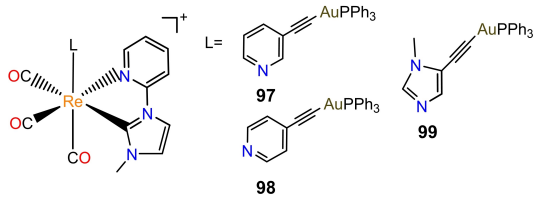

Figure 22. Structures of gold conjugates **97**–**99**.[89]

Fluorescence confocal microscopy studies show that **97** and **98** mostly accumulate within the cytoplasm close to the nucleus with smaller quantities found within the nucleus. Flow cytometry of cells treated with **97** and **98** shows that they are predominately undergoing necrosis. Compared to compounds **87**–**89** bearing the bipyridine ligand, NHC derivatives **97**–**99** exhibit similar cellular localization patterns, cytotoxic activities, and modes of cell death, suggesting that the NHC ligand does not play a significant role in influencing the biological properties of these compounds.

As an alternative to attaching the Au(I)-alkynyl fragments to the axial position of the $Re(CO)_3$ core, these fragments were conjugated to the equatorial bipyridine ligand in compounds **100**–**104** (Figure 23).[90] The cationic complexes **103** and **104**, in which the $Re(CO)_3$ core bears an acetonitrile ligand, are more cytotoxic than the neutral ones **100**–**102**, in which the Re center contains an axial chloride. The enhanced cytotoxicity of the cationic complexes **103** and **104** may be attributed to their higher solubility and greater cellular uptake. Moreover, fluorescence microscopy studies revealed that in A549 lung cancer cells, **103** and **104** were randomly distributed in the outside of the cell in the form of precipitate, whereas in HeLa cervical cancer cells, the same complexes were located close to the cellular membrane. These observations possibly explain their higher cytotoxicity against HeLa cells with respect to A549 cells. Compared to compounds **87**–**89** where alkynyl Au(I) is linked to the axial position of the $Re(CO)_3$ core, complexes **100**–**104** exhibit lower cytotoxic activity and unfavorable cellular localization, suggesting that axial conjugation is the better strategy for designing this class of compounds for biological applications.

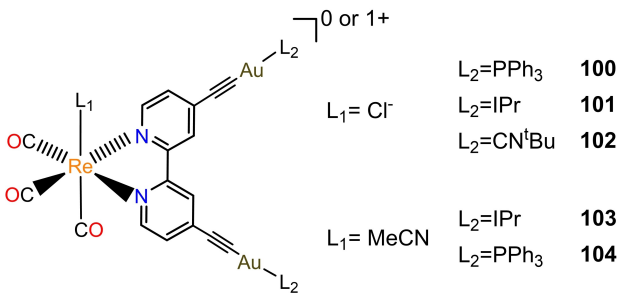

Figure 23. Structures of gold conjugates **100**–**104**.[90]

3.4. Rare Earth Metals

The rare earth elements, or lanthanides, have useful diagnostic applications because their contracted 4f orbitals can give rise to novel magnetic and spectroscopic properties, which can be leveraged for both magnetic resonance imaging (MRI) and photoluminescent imaging applications.[91] Although several $Re(CO)_3$ conjugates with photoluminescent lanthanides have been reported, these compounds have been evaluated primarily to assess their fundamental photophysical properties rather than their potential biological applications.[92] By contrast, several different Re-Gd conjugates have been prepared and tested as dual imaging probes, using the photoluminescent ^{3}MLCT state of the $Re(CO)_3$ core and the $S = 7/2$ magnetic ground state of the Gd^{3+} ion. Compound **105**, for example, contains a Gd-DOTA complex attached to the $Re(CO)_3$ core via an axial pyridine linkage (Figure 24). The photoluminescence lifetime of **105** is 0.12 μs, much longer than the corresponding mononuclear Re compound, $[Re(CO)_3bpyCl]$ (< 10 ns).[93] Furthermore, the relaxivity of **105** is 3.9 $mM^{-1}s^{-1}$ in aqueous buffer, comparable to that of the mononuclear gadolinium complex (4.5 $mM^{-1}s^{-1}$).

Another Re-Gd conjugate, compound **106**, uses an acyclic ligand to contain the Gd^{3+} center, which is still attached to the axial position of the $Re(CO)_3$ core (Figure 24).[94,95] Notably, in H_2O at physiological pH, **106** has a relaxivity that is 1.7–1.9 times higher than those of $[Gd(DTPA)(H_2O)]^{2-}$ and $[Gd(DOTA)(H_2O)]^-$, which are MRI contrast agents currently used in clinical practice. Additionally, compound **106** is luminescent with a quantum yield of 1.4% in aqueous solution.

4. Conclusions

In this Minireview, we provide an overview of both homonuclear and heteronuclear multimetallic $Re(CO)_3$ complexes that have been investigated for biomedical applications. For the homonuclear complexes, a number of examples demonstrated that multinuclearity could improve cellular uptake by increasing

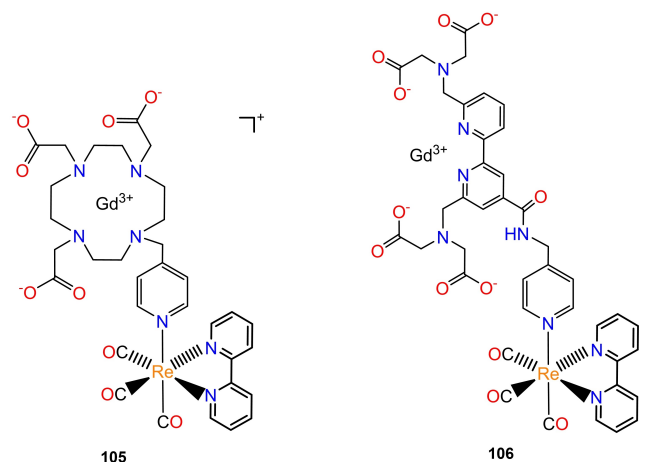

Figure 24. Structures of gadolinium conjugates **105** and **106**.[93–95]

the complex lipophilicity or charge. In turn enhanced cytotoxicity and cellular imaging properties could be observed. With respect to the cytotoxicity enhancement, however, a comparison to the corresponding mononuclear analogues should be made, in order to assess whether such enhancement is synergistic or simply additive on a per metal basis.

For heteronuclear complexes, $Re(CO)_3$ was primarily employed as an imaging modality in several different contexts. First, the photoluminescent properties of the $Re(CO)_3$ diimmine moiety make it suitable as an supplemental luminophore for other non-emissive metallodrugs, as demonstrated by the multiple examples of Re-Au conjugates that were discussed. Second, the $Re(CO)_3$ diimine moiety can be combined with other established imaging agents to form "dual-imaging probes", as evidenced by the reports of Re-Tc and Re-Gd complexes. Lastly, even when the $Re(CO)_3$ fragment is non-emissive or the luminescence is quenched by other parts of the conjugates, its signature IR stretching modes can still provide valuable information on cellular environments via vibrational imaging, as shown by the studies on Re-cobalamin and Re-Fc conjugates.

When $Re(CO)_3$ is employed as a therapeutic component in heteronuclear complexes, its role is somewhat more ambiguous. There are cases where the addition of Re to another metallodrug reduces the overall complex cytotoxicity. Additionally, the stability of heterometallic complexes under physiological conditions is often not examined, which makes it difficult to tell whether the activity comes from the intact complex or individual mononuclear fragments. Perhaps more importantly, there is a lack of investigation on the mechanism of action of heterometallic anticancer complexes in general.[29] Because of the paucity of the studies mentioned above, many compounds are arbitrarily prepared rather than rationally designed.

In any case, numerous fundamentally interesting compounds with increased functionality discussed above highlight that there is still much potential for $Re(CO)_3$-based multimetallic complexes as therapeutic and diagnostic agents, given the favorable photophysical properties and unique modes of action of $Re(CO)_3$ moieties. For future studies, an emphasis should be put on the rational design and mechanistic understanding of the multimetallic complexes.

Acknowledgements

This work was supported in part by the College of Arts and Sciences at Cornell University.

Conflict of Interest

The authors declare no conflict of interest.

Keywords: Anticancer agents · Bioinorganic chemistry · Imaging probes · Metallodrugs · Multimetallic complexes

[1] K. K.-W. Lo, K. Y. Zhang, S. P.-Y. Li, *Eur. J. Inorg. Chem.* **2011**, *2011*, 3551–3568.
[2] A. Leonidova, G. Gasser, *ACS Chem. Biol.* **2014**, *9*, 2180–2193.
[3] S. Hostachy, C. Policar, N. Delsuc, *Coord. Chem. Rev.* **2017**, *351*, 172–188.
[4] L. C.-C. Lee, K.-K. Leung, K. K.-W. Lo, *Dalton Trans.* **2017**, *46*, 16357–16380.
[5] C. C. Konkankit, S. C. Marker, K. M. Knopf, J. J. Wilson, *Dalton Trans.* **2018**, *47*, 9934–9974.
[6] E. B. Bauer, A. A. Haase, R. M. Reich, D. C. Crans, F. E. Kühn, *Coord. Chem. Rev.* **2019**, *393*, 79–117.
[7] P. Collery, D. Desmaele, V. Vijaykumar, *Curr. Pharm. Des.* **2019**, *25*, 3306–3322.
[8] I. Kitanovic, S. Can, H. Alborzinia, A. Kitanovic, V. Pierroz, A. Leonidova, A. Pinto, B. Spingler, S. Ferrari, R. Molteni, A. Steffen, N. Metzler-Nolte, S. Wölfl, G. Gasser, *Chem. Eur. J.* **2014**, *20*, 2496–2507.
[9] S. Imstepf, V. Pierroz, R. Rubbiani, M. Felber, T. Fox, G. Gasser, R. Alberto, *Angew. Chem. Int. Ed.* **2016**, *55*, 2792–2795; *Angew. Chem.* **2016**, *128*, 2842–2845.
[10] P. V. Simpson, I. Casari, S. Paternoster, B. W. Skelton, M. Falasca, M. Massi, *Chem. Eur. J.* **2017**, *23*, 6518–6521.
[11] K. M. Knopf, B. L. Murphy, S. N. MacMillan, J. M. Baskin, M. P. Barr, E. Boros, J. J. Wilson, *J. Am. Chem. Soc.* **2017**, *139*, 14302–14314.
[12] M. König, D. Siegmund, L. J. Raszeja, A. Prokop, N. Metzler-Nolte, *MedChemComm* **2018**, *9*, 173–180.
[13] M. Muñoz-Osses, F. Godoy, A. Fierro, A. Gómez, N. Metzler-Nolte, *Dalton Trans.* **2018**, *47*, 1233–1242.
[14] L. He, Z.-Y. Pan, W.-W. Qin, Y. Li, C.-P. Tan, Z.-W. Mao, *Dalton Trans.* **2019**, *48*, 4398–4404.
[15] C. C. Konkankit, B. A. Vaughn, S. N. MacMillan, E. Boros, J. J. Wilson, *Inorg. Chem.* **2019**, *58*, 3895–3909.
[16] A. P. King, S. C. Marker, R. V. Swanda, J. J. Woods, S.-B. Qian, J. J. Wilson, *Chem. Eur. J.* **2019**, *25*, 9206–9210.
[17] S. C. Marker, A. P. King, R. V. Swanda, B. Vaughn, E. Boros, S.-B. Qian, J. J. Wilson, *Angew. Chem. Int. Ed.* **2020**, *59*, 13391–13400.
[18] S. C. Marker, A. P. King, S. Granja, B. Vaughn, J. J. Woods, E. Boros, J. J. Wilson, *Inorg. Chem.* **2020**, *59*, 10285–10303.
[19] K. Wähler, A. Ludewig, P. Szabo, K. Harms, E. Meggers, *Eur. J. Inorg. Chem.* **2014**, *2014*, 807–811.
[20] A. Leonidova, V. Pierroz, R. Rubbiani, J. Heier, S. Ferrari, G. Gasser, *Dalton Trans.* **2014**, *43*, 4287–4294.
[21] E. Kottelat, V. Chabert, A. Crochet, K. M. Fromm, F. Zobi, *Eur. J. Inorg. Chem.* **2015**, *2015*, 5628–5638.
[22] I. Chakraborty, S. J. Carrington, G. Roseman, P. K. Mascharak, *Inorg. Chem.* **2017**, *56*, 1534–1545.
[23] S. C. Marker, S. N. MacMillan, W. R. Zipfel, Z. Li, P. C. Ford, J. J. Wilson, *Inorg. Chem.* **2018**, *57*, 1311–1331.
[24] I. Maisuls, F. M. Cabrerizo, P. M. David-Gara, B. Epe, G. T. Ruiz, *Chem. Eur. J.* **2018**, *24*, 12902–12911.
[25] L. Quaroni, F. Zobi, in *Inorganic Chemical Biology: Principles, Techniques and Applications* (Ed.: G. Gasser), John Wiley & Sons, Chichester, **2014**, pp. 137–170.
[26] S. Clède, C. Policar, *Chem. Eur. J.* **2015**, *21*, 942–958.
[27] S. Jürgens, W. A. Herrmann, F. E. Kühn, *J. Organomet. Chem.* **2014**, *751*, 83–89.
[28] E. Boros, A. B. Packard, *Chem. Rev.* **2019**, *119*, 870–901.
[29] A. van Niekerk, P. Chellan, S. F. Mapolie, *Eur. J. Inorg. Chem.* **2019**, *2019*, 3432–3455.
[30] V. Fernández-Moreira, M. C. Gimeno, *Chem. Eur. J.* **2018**, *24*, 3345–3353.
[31] S. Pete, N. Roy, P. Paira, *Inorg. Chim. Acta* **2020**, *517*, 120184.
[32] J. F. Berry, C. M. Thomas, *Dalton Trans.* **2017**, *46*, 5472–5473.
[33] E. M. Hahn, A. Casini, F. E. Kühn, *Coord. Chem. Rev.* **2014**, *276*, 97–111.
[34] R. G. Balasingham, F. L. Thorp-Greenwood, C. F. Williams, M. P. Coogan, S. J. A. Pope, *Inorg. Chem.* **2012**, *51*, 1419–1426.
[35] A. W.-T. Choi, K. K.-S. Tso, V. M.-W. Yim, H.-W. Liu, K. K.-W. Lo, *Chem. Commun.* **2015**, *51*, 3442–3445.
[36] B. L. Oliveira, Z. Guo, G. J. L. Bernardes, *Chem. Soc. Rev.* **2017**, *46*, 4895–4950.
[37] R.-R. Ye, C.-P. Tan, M.-H. Chen, L. Hao, L.-N. Ji, Z.-W. Mao, *Chem. Eur. J.* **2016**, *22*, 7800–7809.
[38] Z.-Y. Pan, D.-H. Cai, L. He, *Dalton Trans.* **2020**, *49*, 11583–11590.
[39] F.-X. Wang, J.-H. Liang, H. Zhang, Z.-H. Wang, Q. Wan, C.-P. Tan, L.-N. Ji, Z.-W. Mao, *ACS Appl. Mater. Interfaces* **2019**, *11*, 13123–13133.
[40] D. Giffard, E. Fischer-Fodor, C. Vlad, P. Achimas-Cadariu, G. S. Smith, *Eur. J. Med. Chem.* **2018**, *157*, 773–781.

[41] C. Ashok Kumar, S. Karthikeyan, B. Varghese, V. Veena, N. Sakthivel, B. Manimaran, *J. Organomet. Chem.* **2014**, *766*, 86–94.
[42] R. Govindarajan, R. Nagarajaprakash, V. Veena, N. Sakthivel, B. Manimaran, *Polyhedron* **2018**, *139*, 229–236.
[43] B. Ramakrishna, R. Nagarajaprakash, V. Veena, N. Sakthivel, B. Manimaran, *Dalton Trans.* **2015**, *44*, 17629–17638.
[44] M. Karthikeyan, R. Govindarajan, E. Duraisamy, V. Veena, N. Sakthivel, B. Manimaran, *ChemistrySelect* **2017**, *2*, 3362–3368.
[45] J. Delasoie, A. Pavic, N. Voutier, S. Vojnovic, A. Crochet, J. Nikodinovic-Runic, F. Zobi, *Eur. J. Med. Chem.* **2020**, *204*, 112583.
[46] S. V. Kumar, W. K. C. Lo, H. J. L. Brooks, L. R. Hanton, J. D. Crowley, *Aust. J. Chem.* **2016**, *69*, 489–498.
[47] M. L. Low, G. Paulus, P. Dorlet, R. Guillot, R. Rosli, N. Delsuc, K. A. Crouse, C. Policar, *BioMetals* **2015**, *28*, 553–566.
[48] A. Palmioli, A. Aliprandi, D. Septiadi, M. Mauro, A. Bernardi, L. De Cola, M. Panigati, *Org. Biomol. Chem.* **2017**, *15*, 1686–1699.
[49] E. Ferri, D. Donghi, M. Panigati, G. Prencipe, L. D'Alfonso, I. Zanoni, C. Baldoli, S. Maiorana, G. D'Alfonso, E. Licandro, *Chem. Commun.* **2010**, *46*, 6255–6257.
[50] G. Mion, T. Gianferrara, A. Bergamo, G. Gasser, V. Pierroz, R. Rubbiani, R. Vilar, A. Leczkowska, E. Alessio, *ChemMedChem* **2015**, *10*, 1901–1914.
[51] F. S. De Rosa, M. V. L. B. Bentley, *Pharm. Res.* **2000**, *17*, 1447–1455.
[52] M. G. H. Vicente, *Curr. Med. Chem. Anti-Cancer Agents* **2001**, *1*, 175–194.
[53] D. E. J. G. J. Dolmans, D. Fukumura, R. K. Jain, *Nat. Rev. Cancer* **2003**, *3*, 380–387.
[54] H. Han, L. H. Hurley, *Trends Pharmacol. Sci.* **2000**, *21*, 136–142.
[55] J. Zhang, J. J. Vittal, W. Henderson, J. R. Wheaton, I. H. Hall, T. S. A. Hor, Y. K. Yan, *J. Organomet. Chem.* **2002**, *650*, 123–132.
[56] W. Wang, Y. K. Yan, T. S. A. Hor, J. J. Vittal, J. R. Wheaton, I. H. Hall, *Polyhedron* **2002**, *21*, 1991–1999.
[57] C. Van Cleave, D. C. Crans, *Inorganics* **2019**, *7*, 111.
[58] F. A. Larik, A. Saeed, T. A. Fattah, U. Muqadar, P. A. Channar, *Appl. Organomet. Chem.* **2017**, *31*, e3664.
[59] M. Wenzel, M. Patra, C. H. R. Senges, I. Ott, J. J. Stepanek, A. Pinto, P. Prochnow, C. Vuong, S. Langklotz, N. Metzler-Nolte, J. E. Bandow, *ACS Chem. Biol.* **2013**, *8*, 1442–1450.
[60] M. Patra, M. Wenzel, P. Prochnow, V. Pierroz, G. Gasser, J. E. Bandow, N. Metzler-Nolte, *Chem. Sci.* **2015**, *6*, 214–224.
[61] J. Oyarzo, A. Acuña, H. Klahn, R. Arancibia, C. P. Silva, R. Bosque, C. López, M. Font-Bardía, C. Calvis, R. Messeguer, *Dalton Trans.* **2018**, *47*, 1635–1649.
[62] Y. Wang, F. Heinemann, S. Top, A. Dazzi, C. Policar, L. Henry, F. Lambert, G. Jaouen, M. Salmain, A. Vessieres, *Dalton Trans.* **2018**, *47*, 9824–9833.
[63] G. Jaouen, A. Vessières, S. Top, *Chem. Soc. Rev.* **2015**, *44*, 8802–8817.
[64] S. Fery-Forgues, B. Delavaux-Nicot, *J. Photochem. Photobiol. A* **2000**, *132*, 137–159.
[65] M. J. Warren, E. Raux, H. L. Schubert, J. C. Escalante-Semerena, *Nat. Prod. Rep.* **2002**, *19*, 390–412.
[66] S. Kunze, F. Zobi, P. Kurz, B. Spingler, R. Alberto, *Angew. Chem. Int. Ed.* **2004**, *43*, 5025–5029; *Angew. Chem.* **2004**, *116*, 5135–5139.
[67] G. Santoro, T. Zlateva, A. Ruggi, L. Quaroni, F. Zobi, *Dalton Trans.* **2015**, *44*, 6999–7008.
[68] A. Boulay, M. Artigau, Y. Coulais, C. Picard, B. Mestre-Voegtlé, E. Benoist, *Dalton Trans.* **2011**, *40*, 6206–6209.
[69] A. François, C. Auzanneau, V. Le Morvan, C. Galaup, H. S. Godfrey, L. Marty, A. Boulay, M. Artigau, B. Mestre-Voegtlé, N. Leygue, C. Picard, Y. Coulais, J. Robert, E. Benoist, *Dalton Trans.* **2014**, *43*, 439–450.
[70] A. Levina, A. Mitra, P. A. Lay, *Metallomics* **2009**, *1*, 458–470.
[71] M. R. Gill, J. A. Thomas, *Chem. Soc. Rev.* **2012**, *41*, 3179–3192.
[72] S. P. Foxon, T. Phillips, M. R. Gill, M. Towrie, A. W. Parker, M. Webb, J. A. Thomas, *Angew. Chem. Int. Ed.* **2007**, *46*, 3686–3688; *Angew. Chem.* **2007**, *119*, 3760–3762.
[73] A. E. Friedman, J.-C. Chambron, J.-P. Sauvage, N. J. Turro, J. K. Barton, *J. Am. Chem. Soc.* **1990**, *112*, 4960–4962.
[74] C. Hiort, P. Lincoln, B. Nordén, *J. Am. Chem. Soc.* **1993**, *115*, 3448–3454.
[75] V. W.-W. Yam, K. K.-W. Lo, K.-K. Cheung, R. Y.-C. Kong, *J. Chem. Soc. Chem. Commun.* **1995**, 1191–1193.
[76] V. W.-W. Yam, K. K.-W. Lo, K.-K. Cheung, R. Y.-C. Kong, *J. Chem. Soc. Dalton Trans.* **1997**, 2067–2072.
[77] H. K. Saeed, S. Sreedharan, P. J. Jarman, S. A. Archer, S. D. Fairbanks, S. P. Foxon, A. J. Auty, D. Chekulaev, T. Keane, A. J. H. M. Meijer, J. A. Weinstein, C. G. W. Smythe, J. Bernardino De La Serna, J. A. Thomas, *J. Am. Chem. Soc.* **2020**, *142*, 1101–1111.
[78] P. J. Jarman, F. Noakes, S. Fairbanks, K. Smitten, I. K. Griffiths, H. K. Saeed, J. A. Thomas, C. Smythe, *J. Am. Chem. Soc.* **2019**, *141*, 2925–2937.
[79] Z.-B. Zheng, Y.-Q. Wu, K.-Z. Wang, F. Li, *Dalton Trans.* **2014**, *43*, 3273–3284.
[80] T. C. Johnstone, K. Suntharalingam, S. J. Lippard, *Chem. Rev.* **2016**, *116*, 3436–3486.
[81] N. Margiotta, N. Denora, S. Piccinonna, V. Laquintana, F. M. Lasorsa, M. Franco, G. Natile, *Dalton Trans.* **2014**, *43*, 16252–16264.
[82] L. Quental, P. Raposinho, F. Mendes, I. Santos, C. Navarro-Ranninger, A. Alvarez-Valdes, H. Huang, H. Chao, R. Rubbiani, G. Gasser, A. G. Quiroga, A. Paulo, *Dalton Trans.* **2017**, *46*, 14523–14536.
[83] B. Bertrand, C. Botuha, J. Forté, H. Dossmann, M. Salmain, *Chem. Eur. J.* **2020**, *26*, 12846–12861.
[84] I. Ott, *Coord. Chem. Rev.* **2009**, *253*, 1670–1681.
[85] B. Bertrand, A. Casini, *Dalton Trans.* **2014**, *43*, 4209–4219.
[86] C. K. Mirabelli, R. K. Johnson, C. M. Sung, L. Faucette, K. Muirhead, S. T. Crooke, *Cancer Res.* **1985**, *45*, 32–39.
[87] V. Fernández-Moreira, I. Marzo, M. C. Gimeno, *Chem. Sci.* **2014**, *5*, 4434–4446.
[88] A. Luengo, V. Fernández-Moreira, I. Marzo, M. C. Gimeno, *Inorg. Chem.* **2017**, *56*, 15159–15170.
[89] A. Luengo, V. Fernández-Moreira, I. Marzo, M. C. Gimeno, *Organometallics* **2018**, *37*, 3993–4001.
[90] A. Luengo, M. Redrado, I. Marzo, V. Fernández-Moreira, M. C. Gimeno, *Inorg. Chem.* **2020**, *59*, 8960–8970.
[91] M. C. Heffern, L. M. Matosziuk, T. J. Meade, *Chem. Rev.* **2014**, *114*, 4496–4539.
[92] S. J. A. Pope, B. J. Coe, S. Faulkner, *Chem. Commun.* **2004**, 1550–1551.
[93] T. Koullourou, L. S. Natrajan, H. Bhavsar, S. J. A. Pope, J. Feng, J. Narvainen, R. Shaw, E. Scales, R. Kauppinen, A. M. Kenwright, S. Faulkner, *J. Am. Chem. Soc.* **2008**, *130*, 2178–2179.
[94] A. Boulay, S. Laine, N. Leygue, E. Benoist, S. Laurent, L. Vander Elst, R. N. Muller, B. Mestre-Voegtle, C. Picard, *Tetrahedron Lett.* **2013**, *54*, 5395–5398.
[95] N. Leygue, A. Boulay, C. Galaup, E. Benoist, S. Laurent, L. Vander Elst, B. Mestre-Voegtlé, C. Picard, *Dalton Trans.* **2016**, *45*, 8379–8393.

Manuscript received: January 15, 2021
Revised manuscript received: February 15, 2021
Accepted manuscript online: February 17, 2021